Driving magnetization perpendicular by antiferromagnetic-ferromagnetic exchange coupling

B. Y. Wang,[1,2] N. Y. Jih,[1] W. C. Lin,[1,3] C. H. Chuang,[1] P. J. Hsu,[1] C. W. Peng,[1] Y. C. Yeh,[1] Y. L. Chan,[4] D. H. Wei,[4] W. C. Chiang,[5] and Minn-Tsong Lin[1,6,*]

[1]*Department of Physics, National Taiwan University, Taipei 106, Taiwan*

[2]*TIGP, Academia Sinica, Taiwan*

[3]*Department of Physics, National Taiwan Normal University, Taipei 106, Taiwan*

[4]*National Synchrotron Radiation Research Center, Hsinchu 300, Taiwan*

[5]*Department of Physics, Chinese Culture University, Taipei 111, Taiwan*

[6]*Institute of Atomic and Molecular Sciences, Academia Sinica, Taipei 106, Taiwan*

(Received 12 January 2011; revised manuscript received 28 January 2011; published 22 March 2011)

Using x-ray photoemission electron microscopy and the magneto-optical Kerr effect, we have demonstrated a perpendicular magnetic anisotropy that could be due to exchange coupling between the ferromagnetic and antiferromagnetic layers. The results of magnetic imaging and hysteresis loops show that the magnetization of Fe and permalloy (Py) films orients from the in-plane to perpendicular direction, as an Mn underlayer is above a threshold value that depends on the Fe or Py layer thickness. Their thickness-dependent behaviors can be quantitatively described by a phenomenological model that takes into account the finite-size effect of the antiferromagnet on exchange coupling. The anisotropy energy extracted from the model and the thermal stability of perpendicular magnetization enhanced with the increase of the Mn underlayer further demonstrate the exchange coupling nature.

DOI: 10.1103/PhysRevB.83.104417 PACS number(s): 75.70.Kw, 75.30.Gw, 75.50.Ee

I. INTRODUCTION

Magnetic anisotropy, which characterizes the preferred orientation of spontaneous magnetization, is one of the most important properties of magnetic materials from both the fundamental and the technological points of view. The importance cannot be overstated, particularly in low-dimensional materials where bits with perpendicular magnetic anisotropy (PMA) are promising building blocks for the out-of-plane type of data storage.[1,2] Naturally, most low-dimensional magnetic materials prefer in-plane magnetization due to shape anisotropy contributed from the dipole-dipole interactions among neighboring magnetic moments. To date, common ways to establish PMA include building periodically alternated ferromagnetic (FM)/noble-metal multilayers which enhance the perpendicular interface anisotropy via modified spin-orbital coupling at the FM/noble-metal interfaces,[3,4] and the use of strained magnetic ultrathin films which exhibit PMA via magnetoelastic coupling.[5–8] On the other hand, antiferromagnetic (AFM) materials are another class of materials of growing practical importance as they play key roles in many state-of-the-art applications in manipulating the magnetization of FM ultrathin films. Through a mechanism known as AFM-FM exchange coupling, AFM materials are commonly used in spin-valves to "pin" the magnetic moment[9] and even to shift the hysteresis loop of the adjacent FM layer by the exchange bias field (H_b) induced at the interfaces.[10]

In this paper, we report that the PMA of FM thin films can be achieved through the mechanism of AFM-FM exchange coupling, presenting another feature of AFM materials, besides the exchange bias coupling.[10] We demonstrate that in a bilayered system, as the AFM layer thickness goes beyond a threshold value, the AFM-FM exchange coupling becomes strong enough to switch the magnetization from an in-plane to perpendicular orientation. Assisted by a simple model and the temperature-dependence data, we reveal that the strength of the PMA is modulated by the Mn thickness (t_{Mn}) according to the finite-size effect of low-dimensional magnetic systems.[11,12] Our work is different from previously reported exchange-biased FM/AFM multilayer systems,[13,14] which showed the induced uniaxial anisotropy energy in coexisting in-plane and perpendicular hysteresis loops, due to a mechanism[13] similar to the FM/noble-metal multilayer systems.[3,4] The finding of a PMA caused by AFM-FM exchange coupling in our work is beyond the current physics of the exchange bias effect, indicating that exchange bias is only one of two effects due to AFM-FM exchange coupling.[15]

II. EXPERIMENT

The magnetic ultrathin films were prepared *in situ* and subsequently investigated in a multifunctional UHV chamber with a base pressure $\sim 2 \times 10^{-10}$ torr. For element-resolved magnetic domain imaging, the chamber was connected to the x-ray magnetic circular dichroism–photoemission electron microscope (XMCD-PEEM) at beamline BL05B2 of NSRRC in Hsinchu, Taiwan, using a commercially available PEEM (Focus IS-PEEM). The $Cu_3Au(001)$ single-crystal substrates with 0.1° miscut were cleaned using cycles of 2 keV Ar ion sputtering. After the ion sputtering, the substrates were annealed at 765 K for 5 minutes and at 645 K for another 30 minutes to obtain well-ordered $C(2 \times 2)$ structure. The ultrathin FM (Fe or Py) and Mn films were deposited at 300 K by thermal evaporation onto $Cu_3Au(001)$ substrates with deposition rates ranging from 60 to 80 seconds/ML.

For different experimental purposes, both uniform bilayered structures and samples with a wedge-shaped Mn underlayer were prepared. The uniform bilayered structures can be applied to various measurements. During the deposition of the uniform films, the film structure and the growth rate were monitored by medium energy electron diffraction (MEED).

Nevertheless, the magnetic anisotropy of the FM/Mn bilayers can be very sensitive to small variations of t_{Mn}. Thus, a sample with a small and continuous variation of t_{Mn} is necessary and can be achieved by using a proper "wedged" Mn underlayer. Together with the XMCD-PEEM measurement (with its capability in sensing magnetic properties with microscopic-scale resolution), the wedged sample has the advantage of allowing us to probe the change of magnetic anisotropy (magnetization direction) of the FM domain in response to the small and continuous variation of t_{Mn}. Such measurement is difficult and inefficient by using an Mn underlayer of uniform thickness. For the preparation of the wedged Mn underlayer, a specially designed shutter was placed close to the substrate. During the deposition process, the evaporation flux was directed normal to the substrate surface to avoid the shadowing effect as the shutter was in place. The thickness and the slope of the wedged Mn underlayer were set by the choice of a suitable deposition rate, as well as by the precise, stepping-motor controlled motion of the substrate. The systematic error of the thickness of the wedged Mn underlayer was about 10%, whereas the thickness deviation within the same sample was smaller than 2%.

To characterize the deposited thin films, Auger electron spectroscopy (AES) was used to detect the surface element and possible contamination. The surface morphology of the ultrathin films was measured by scanning tunneling microscopy (STM),[16] and the average interlayer distance was estimated by analyzing the low-energy electron diffraction (LEED) spectrum using the kinematics approximation (LEED I/V).[7,17–19] Although a more sophisticated dynamic LEED technique is available,[20] the kinematic LEED analysis has been widely accepted to effectively monitor the average vertical lattice structure of the deposited films. In the relevant case of Fe/Cu_3Au(001), kinematic LEED is shown to be a reliable technique providing results consistent with most works[21–24] of different groups using various techniques. For the magnetic properties, the magneto-optical Kerr effect (MOKE), assisted by the lock-in technique, of both longitudinal and polar geometries, was used to measure the hysteresis loops of the magnetic thin films. To obtain the exchange bias field, some specific samples were treated with a perpendicularly oriented field cooling process, in which the sample was cooled down from room temperature to 240 K with a 600 Oe external field.

Synchrotron radiation XMCD-PEEM[25,26] was adopted for element-resolved magnetic domain imaging. With XMCD, the magnetism information of each element can be obtained from the asymmetry of left and right circularly polarized (LCP and RCP) x-ray absorption spectra (XAS) at the characteristic absorption energies. Combining XMCD and PEEM, the full-field view of the emitted secondary electrons from the magnetic sample can be resolved by a CCD camera through the use of a multichannel plate. Since the absorption intensity depends on the relative orientation between the polarization of the x-ray and the magnetization direction, the areas showing different gray levels indicate magnetic domains of different magnetization directions. The direction of domain magnetization can thus be resolved by observing the variation of the gray-level contrast while rotating the sample around the azimuth axis. Samples with a wedge-shaped Mn underlayer, deposited on Cu_3Au(001), were used for XMCD-PEEM imaging. The incident angle of x rays was 65° from the surface normal. The wavelength of the incident x rays was tuned to the maximal resonance of the L_3 and the L_2 absorption edges of Fe (or Mn) to obtain the element-resolved magnetic contrast. Images with magnetic contrast were constructed by dividing the two full-field images, taken at the Fe (or Mn) L_3 and L_2 edges, utilizing the absorption asymmetry at the L edges.

III. RESULTS

A. Crystalline structure and interface properties of Fe, Py/Mn/Cu_3Au(001)

The crystalline structures were confirmed by LEED and LEED I/V as described in the previous section. Room temperature deposition of Mn ultrathin films on Cu_3Au(001) leads to layer-by-layer growth with smooth surfaces and face-centered-cubic (fcc)–like crystalline structure.[16] Two different FM films, i.e., body-centered-tetragonal (bct) Fe and fct permalloy (Py), were grown on the Mn underlayer.

The crystalline structure of the Fe overlayer continues to replicate that of the Mn underlayer at low coverage. However, regardless of the presence of the Mn underlayer, the Fe film grown on Mn/Cu_3Au(001) undergoes structural transition from fcc to bct starting at an Fe layer thickness (t_{Fe}) near 3 ML, and reveals an invariant bct structure as t_{Fe} becomes larger than 3.6 ML. Figures 1(a) and 1(c) show the LEED specular spot I/V curves and the interlayer distance of 6 ML Fe/n ML Mn/Cu_3Au(100), respectively. The 6 ML Fe films reveal bct structure and remain invariant while grown on fcc-Mn underlayers with different thicknesses. As the temperature is varied from 100 K to 300 K, the interlayer distance of the 6 ML Fe films expands only a tiny amount (from 1.55 ± 0.01 Å to 1.56 ± 0.01 Å), as shown in Figs. 1(b) and 1(d). Although a more significant temperature effect on structure was reported by Bisio *et al.*,[27] the effect was observed only in a higher temperature range (345 $\sim$ 380 K). Thus, in the present work within a temperature range of 220 K $\leqslant T \leqslant$ 260 K, the influence of temperature variation on magnetic properties of thin films via structure transition is minor. As t_{Fe} continues to expand, the Fe film relaxes gradually from bct to bcc structure. For Fe films grown on 0, 4, 8, and 15 ML Mn/Cu_3Au(100) [shown in Fig. 1(e)], the t_{Fe} increases from 4.5 ML to 14 ML, corresponding to a c/a ratio varying from 1.17 to 1.08, following the bct-bcc relaxation trend and the so-called epitaxial curve predicated by theoretical calculation.[28] These c/a values were also used to estimate the related magnetic energy term in the following theoretical analysis.

On the other hand, the Py films shown in Fig. 2 exhibit a fct structure for the entire thickness range, regardless of the presence of the Mn underlayer. Thus, both FM films reveal a common behavior in which the structures are invariant upon varying the Mn underlayer thickness. For the interface properties, according to our previous study[16] with AES and MOKE, the magnetic "dead layer" resulting from the intermixing or antiparallel coupled Fe-Mn magnetic moments at the Fe/Mn interface is less than 2 ML. Therefore, the reduced (in-plane) shape anisotropy due to magnetic frustration caused by the intermixing of Fe/Mn should not be strong enough to switch the magnetization orientation of the Fe layer at

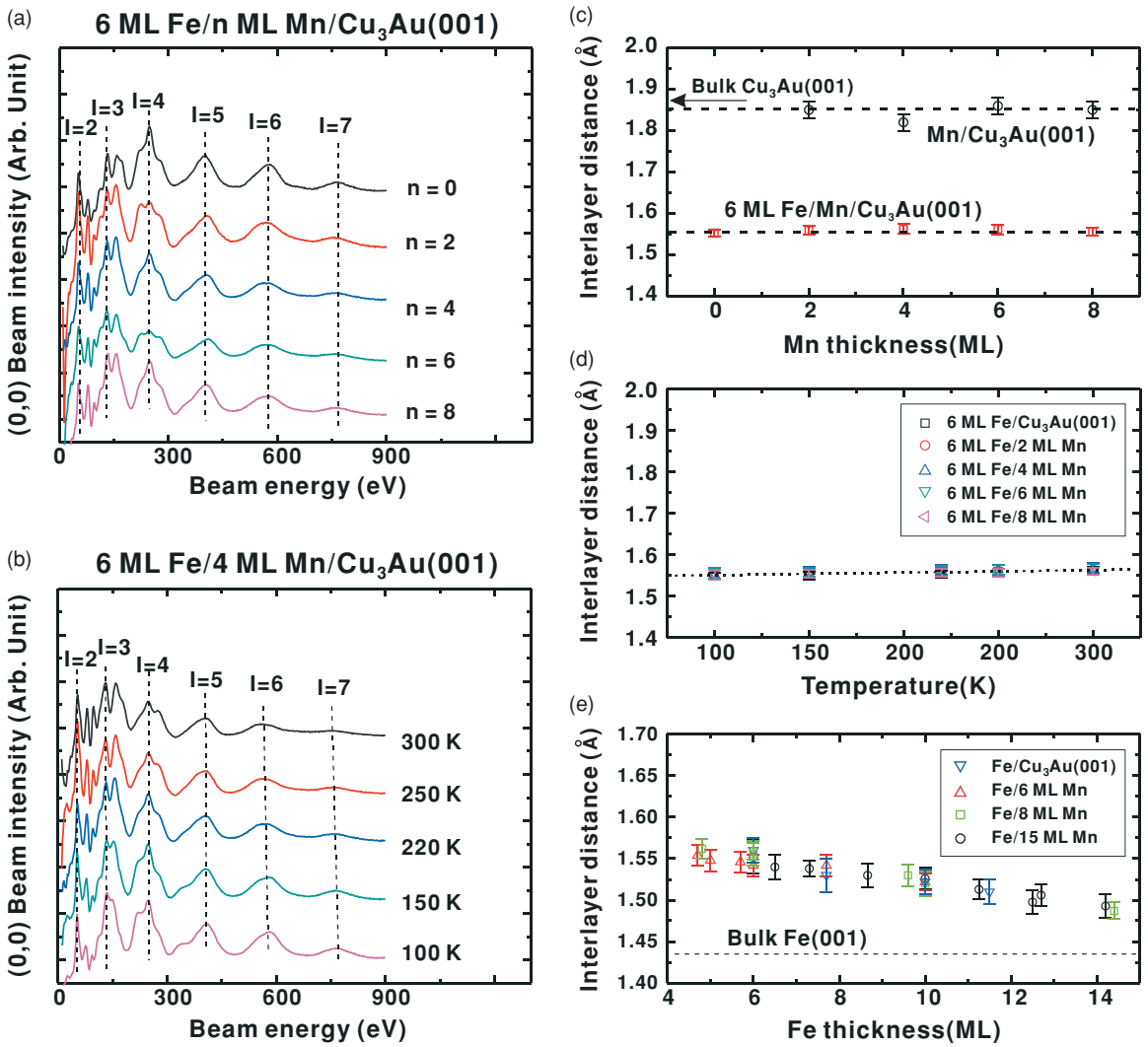

FIG. 1. (Color online) Interlayer distances of uniform Fe/Mn/Cu_3Au(001) bilayers with different t_{Mn} and t_{Fe}, measured at various temperatures. (a) Selected LEED specular spot I/V curves for 6 ML Fe/*n* ML Mn/Cu_3Au(100) measured at 220 K. (b) I/V curves for 6 ML Fe/4 ML Mn/Cu_3Au(100) measured at various temperatures. The dashed lines index the maximum condition for the Bragg interference. (c) Interlayer distances of 6 ML Fe on *n* ML Mn/Cu_3Au(100) calculated from (a) and *n* ML Mn on Cu_3Au(100) measured at 100 K. The 6 ML Fe films reveal bct structure and remain invariant when grown on fcc-Mn underlayers of different thickness. (d) Temperature-dependent interlayer distances of 6 ML Fe on *n* ML Mn/Cu_3Au(100). For all 6 ML Fe films, the interlayer distance expands slightly from 1.55 ± 0.01 Å to 1.56 ± 0.01 Å as temperature is increased from 100 K to 300 K. (e) Summarized interlayer distances of various Fe films on 0, 4, 8, and 15 ML Mn/Cu_3Au(100).

larger coverage. Thus, the results presented above indicate that significant structural or intermixing effects on the magnetic properties of FM/Mn bilayers can be excluded.

B. Magnetic domain imaging on 6 ML Fe/wedged-Mn/Cu_3Au(001)

Since the magnetic anisotropy of FM/Mn bilayers can be very sensitive to the variation of t_{Mn}, the investigation was first performed on a uniform 6 ML Fe film with a wedge-shaped Mn underlayer, utilizing the XMCD-PEEM magnetic imaging.[25,26] Figure 3(a) shows the Fe domain image of 6 ML Fe/wedged-Mn/Cu_3Au(001), with incoming x rays of left-circular polarization (LCP). The sample is further precessed 180° along the [001] direction to let the incident x-rays on the sample in Fig. 3(b), as compared with 3(a), have the same perpendicular projection of photohelicity ($\sigma_\perp$) but inverse in-plane projection of photohelicity ($\sigma_\parallel$). Thus, for Figs. 3(b) and 3(a), the magnetic domains showing inverse contrast in the region of $t_{Mn} < 2$ ML present the signature of in-plane anisotropy. The slight difference of magnetic contrast in $t_{Mn} > 2$ ML might result from the canted orientation or background variation in both measurements. However, a better gray-level or magnetic contrast can be obtained by subtracting the two images acquired at L_3 with different helicities [as shown in Fig. 3(d)], such that the inhomogeneity of the incident light at different L_3 and L_2 energy edges can be eliminated. On the other hand, we keep the same instrument configuration as in Fig. 3(b) but reverse the polarization of the incident x rays from left- to right-circular

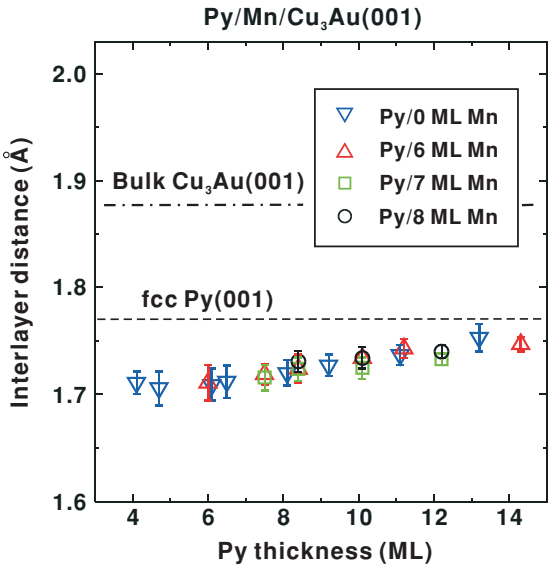

FIG. 2. (Color online) The interlayer distances of Py films on $Mn/Cu_3Au(001)$. The interlayer distance of Py films varies from 1.71 Å to 1.75 Å with t_{Py} increased from 4.0 to 14.3 ML, revealing fct-like structure. For Py film at specific thickness, its interlayer distance remains invariant while grown on Mn layers with different thicknesses.

polarization (RCP), as shown in Fig. 3(c). This makes the incident x rays of the sample in Fig. 3(c) have the same $\sigma_{\parallel}$ but inverse $\sigma_{\perp}$ with that in Fig. 3(a). By comparing Fig. 3(c) with 3(a), an inverse domain contrast shown in the region of $t_{Mn} > 2$ ML presents the characteristics of PMA. Thus, with the comparison of Figs. 3(a)–3(d), we have demonstrated a magnetization switching from the in-plane to perpendicular direction in the 6 ML Fe/wedged-Mn bilayer with the increase of t_{Mn}, showing a behavior known as the spin-reorientation transition (SRT).

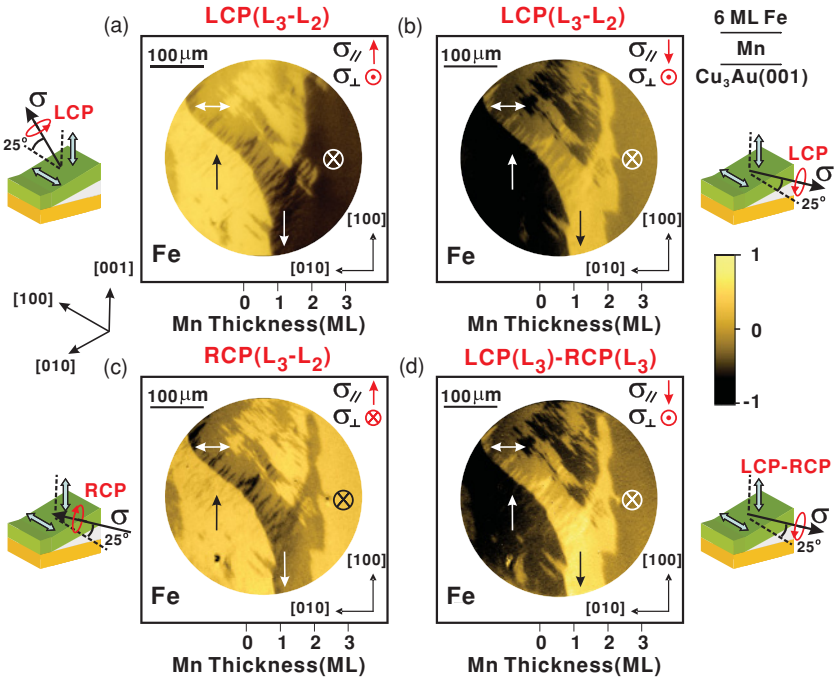

FIG. 3. (Color online) Fe magnetic domain images of 6 ML Fe/wedged-Mn/$Cu_3Au(001)$, measured at 220 K. (a), (b), and (c) show the images with different photohelicity (σ) of incident x rays on the same sample, as indicated in the corresponding cartoons and figures. The contrast of Fe domains changes sensitively with the inversion of $\sigma_{\parallel}$ for $t_{Mn} < 2$ ML and $\sigma_{\perp}$ for $t_{Mn} > 2$ ML, demonstrating a magnetization switching from in-plane to perpendicular with a critical thickness of $t_{Mn} \sim 2$ ML. (d) Shows the image taken with LCP-RCP at the L_3 edge as a comparison.

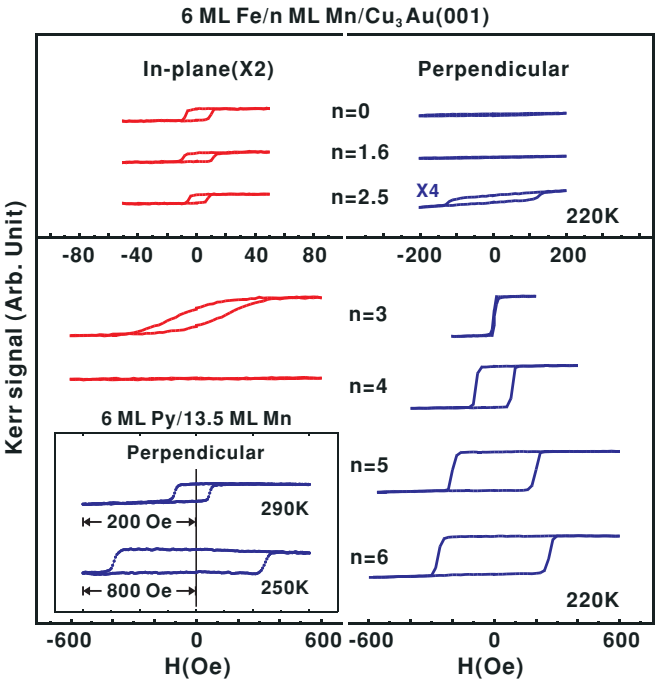

FIG. 4. (Color online) Hysteresis loops for a series of uniform 6 ML Fe/Mn/$Cu_3Au(001)$ with various t_{Mn}, measured at 220 K. The PMA of the Fe layer is enhanced with increasing Mn thickness. The inset shows the hysteresis loops for 6 ML Py/13.5 ML $Mn/Cu_3Au(001)$ measured at 250 K and 290 K after perpendicular field cooling, in which the Mn layer is strong enough to induce both PMA and exchange bias field.

C. Enhanced perpendicular magnetic anisotropy and magnetic phase diagrams of Fe, Py/Mn/$Cu_3Au(001)$

Moreover, we have also investigated the macroscopic magnetic behavior by performing the MOKE measurements on a series of 6 ML Fe/Mn/$Cu_3Au(001)$ (nonwedged) at 220 K, as shown in Fig. 4. Consistent with the XMCD-PEEM results, the

magnetization of the 6 ML Fe/Mn/Cu_3Au(001) series is also found to switch from the in-plane to perpendicular direction at t_{Mn} around 2.5 ML. In perpendicular hysteresis loops, we found that the coercive field (H_c) increases drastically from 10 Oe to 250 Oe as t_{Mn} changes from 3 ML to 6 ML. This enhancement of H_c is conventionally regarded as a fingerprint of the AFM-FM exchange coupling.[10] In 6 ML Fe/Mn/Cu_3Au(001), the increase of t_{Mn} results in the occurrence of PMA, accompanied by the enhancement of H_c, indicating that the mechanism causing the PMA of the Fe/Mn bilayer system is likely associated with the AFM-FM exchange coupling. It is noted that no H_b was observed in 6 ML Fe/Mn/Cu_3Au(100) with present perpendicular field cooling condition. Nevertheless, after replacing Fe by soft magnetic Py, a perpendicular H_b was observed at t_{Mn} = 13.5 ML, as shown in inset of Fig. 4. This indicates the exchange coupling could cause the PMA of 6 ML Fe/Mn/Cu_3Au(001) as shown in Fig. 4, but not strongly enough to induce an exchange bias field.[15]

To obtain a global analysis of the magnetization behavior of both Fe/Mn and Py/Mn bilayers, we extended the hysteresis-loop measurements to include the variation of FM and Mn layer thicknesses, and summarized the results in two magnetic phase diagrams (see Fig. 5). In Fig. 5(a), the PMA of Fe/Mn/Cu_3Au(001) is observed for $t_{Fe} \leqslant 3$ ML. This result is consistent with the Fe/Cu_3Au(001) system which exhibits PMA for $t_{Fe} \leqslant 3.6$ ML.[18] However, depending on t_{Mn}, the range of t_{Fe} within which PMA can be achieved extends from 3 ML to 8 ML. A thicker Mn layer is found capable of stabilizing the PMA for a thicker Fe layer. Similar results can be found in Fig. 5(b) for Py/Mn/Cu_3Au(001). Without the Mn underlayer, the Py films reveal only in-plane anisotropy. This is consistent with earlier studies of fcc-like Py films.[29,30] Nevertheless, we are still able to obtain PMA and the corresponding H_c enhancement in the Py bilayered system with $t_{Mn} > 4$ ML, implying also a correlation with the AFM-FM exchange coupling.[10]

D. Correlation of PMA and AFM-FM exchange coupling investigated with phenomenological model

To clarify the connection between the PMA and AFM-FM exchange coupling as well as the AFM nature of the Mn underlayer, we performed a quantitative analysis using a simple Néel type phenomenological model that includes finite-size scaling for the ultrathin AFM layer.[31–33] The prototype model treats the magnetic anisotropy energy (E_a) of a magnetic thin film as contributed from two terms, i.e., the surface and the volume terms, as follows:[31,32]

$$E_a = \left[\frac{2K_s}{t_{FM}} + (K_{me} - 2\pi M^2)\right] \sin^2\theta, \qquad (1)$$

where θ is the angle between the magnetization vector and the surface normal. Therefore the angle corresponding to the minimum E_a describes the magnetic easy axis of the magnetic thin film. $2K_s$ is the interface anisotropy energy contributed from two interfaces. t_{FM} is the thickness of the FM layer. The volume anisotropy energy contains both magnetoelastic anisotropy energy (K_{me}) and shape anisotropy energy ($K_{shape} = -2\pi M^2$), where M is the magnetic moment density.

For AFM-FM exchange-coupled bilayers, the magnetic anisotropy energy of the FM layer can also be influenced by AFM-FM exchange coupling which is modulated by variation of the AFM thickness. To describe this effect, the Néel type model is generalized by including the finite-size scaling formula in the ultrathin limit[33,34] as follows:

$$\frac{T_{ordering}(\infty) - T_{ordering}(t)}{T_{ordering}(t)} = \left(\frac{\xi}{t}\right)^{\lambda}. \qquad (2)$$

In the original case, finite-size scaling describes the magnetic ordering temperature $T_{ordering}$ like the Curie temperature T_C or Néel temperature T_N for FM or AFM alone,[11,33–35] respectively. The shift in $T_{ordering}$ with thickness variation t is given by the effective-shift exponent (λ) and the spin-correlation length (ξ). For AFM-FM exchange bias coupled systems, it was reported that the trend of T_N decreases with the increase of AFM thickness,[36] which is contrary to the prediction of finite-size scaling. However, in Ref. 37 it was concluded that, instead of T_N, the blocking temperature T_B should be a much better physical quantity to describe the strength of unidirectional AFM-FM exchange coupling (exchange bias) and the corresponding AFM ordering.

Indeed, T_B following with finite-size scaling has been confirmed by numerous studies in various FM/AFM bilayers.[12,38–40] This relation has also been applied in NiFe/IrMn exchange biased bilayers to describe the AFM anisotropy with finite-size scaling.[12] Thus, in the present

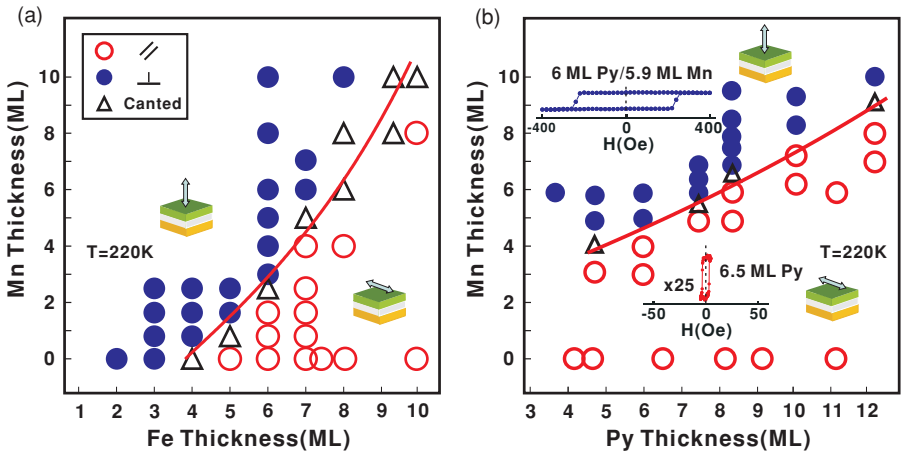

FIG. 5. (Color online) Magnetic phase diagrams for (a) Fe/Mn/Cu_3Au(001) and (b) Py/Mn/Cu_3Au(001) with systematic variations of t_{Mn} and $t_{Fe}(t_{Py})$, taken at 220 K. The insets of (b) show the perpendicular (top) and the in-plane (bottom) hysteresis loops of 6 ML Py/5.9 ML Mn/Cu_3Au(001) and 6.5 ML Py/Cu_3Au(001), respectively. The solid lines in both diagrams indicate the SRT boundary fitted by the magnetic anisotropy model.

FM/Mn bilayers, we can assume that the strength of interface anisotropy energy contributed by Mn-FM exchange coupling, namely K_s^{Mn}, is proportional to the corresponding "effective" T_{ordering} of the Mn layer. This allows K_s^{Mn} to be described by the formula of Eq. (2). Thus, the analytic form of the total interface magnetic anisotropy energy of the FM film can be expressed as

$$K_s^0 + K_s^{\mathrm{Mn}} = K_s^0 + K_s^{\mathrm{Bulk\,Mn}} \left[1 + \left(\frac{\xi}{t_{\mathrm{Mn}}} \right)^{\lambda} \right]^{-1}, \qquad (3)$$

where K_s^0 is the "conventional" interface anisotropy constant[41] that includes the interface anisotropy energies (which are t_{Mn} independent) from both interfaces of the FM layer. On the other hand, K_s^{Mn} depends on t_{Mn} and follows the formula of finite-size scaling [Eq. (2)],[33] and $K_s^{\mathrm{Bulk\,Mn}}$ corresponds to the value of K_s^{Mn} for bulk fcc-Mn ($t_{\mathrm{Mn}} \sim \infty$). The effective spin-correlation length ξ and shift exponent λ are characteristic quantities related to the spin-spin interaction length and coupling strength of the Mn film, respectively.[42]

Using Eq. (3) as the surface term of Eq. (1), we can fit the SRT boundaries in both magnetic phase diagrams of Fe/Mn and Py/Mn bilayers [Figs. 5(a) and 5(b)], respectively. For the volume term of Eq. (1), we have $M_{\mathrm{Fe}} = 2.18\ \mu_B/\mathrm{atom}$,[43] $M_{\mathrm{Py}} = 1.00\ \mu_B/\mathrm{atom}$,[43] $2\pi M_{\mathrm{Fe}}^2 = 132\ \mu\mathrm{eV/atom}$, and $2\pi M_{\mathrm{Py}}^2 = 27\ \mu\mathrm{eV/atom}$. For bct-Fe films on Mn/Cu_3Au(001), t_{Fe} changing from 4 to 10 ML results in a *c*/*a* ratio variation from 1.17 to 1.12 which corresponds to K_{me} varying from $-40\ \mu\mathrm{eV/atom}$ to $-52\ \mu\mathrm{eV/atom}$.[44] In contrast, K_{me} of the fct-Py films is neglected due to the low magnetostriction nature of permalloy. According to the interface anisotropy energy terms given by Eq. (3), we include four independent parameters K_s^0, $K_s^{\mathrm{Bulk\,Mn}}$, ξ, and λ with one constraint in each fitting of Fe/Mn/Cu_3Au(001) and Py/Mn/Cu_3Au(001). The fitting parameters K_s^0, $K_s^{\mathrm{Bulk\,Mn}}$, ξ, and λ are $656.0 \pm 15.2\ \mu\mathrm{eV/atom}$, $3023.9 \pm 649\ \mu\mathrm{eV/atom}$, 16.1 ± 5.6 ML, and 1.09 ± 0.09 for Fe/Mn/Cu_3Au(001), and $-68.5 \pm 21.5\ \mu\mathrm{eV/atom}$, $1200 \pm 235\ \mu\mathrm{eV/atom}$, 16.9 ± 4.5 ML, and 1.09 ± 0.13 for Py/Mn/Cu_3Au(001), respectively.

With careful examination, we found that the values of the physical quantities extracted from our fittings are consistent with the values reported in the literature. The value $1/\lambda = 0.91 \pm 0.09$ is close to the theoretical value of 0.9 ± 0.1 for fcc-AFM film based on Monte Carlo simulations.[45] The value $\xi \sim 16$ ML (3 nm) is also consistent with the values of other Mn-based alloys given in the literature[38,40] (see Table I). The value of ξ also predicts that K_s^{Mn} tends to saturate to $K_s^{\mathrm{Bulk\,Mn}}$ while t_{Mn} is ~16 ML [assuming that the influence of the fcc-fct structural transition of Mn/Cu_3Au(001) on the contribution of PMA is minor]. It is noticed that the common values of shift exponent λ (~1.09) and spin-correlation length ξ (~16 ML) of Mn shard by Fe/Mn and Py/Mn bilayer systems supports the similar AFM natures of the Mn layer in these two systems. On the other hand, K_s^0 describes the intrinsic interface anisotropy energy of bct-Fe or fct-Py film. The value $1.70 \pm 0.04\ \mathrm{mJ/m^2}$ (~$656\ \mu\mathrm{eV/atom}$) for Fe and $-0.177 \pm 0.056\ \mathrm{mJ/m^2}$ (~$-68\ \mu\mathrm{eV/atom}$) for Py films are consistent with the reported values $1.40 \sim 1.88\ \mathrm{mJ/m^2}$ (Refs. 46–53) and $-0.220\ \mathrm{mJ/m^2}$ (Refs. 29,30), respectively (see Table II).

TABLE I. Effective spin-correlation length of various AFM layers.

System	ξ (nm)	Method
fcc-Mn (Fe)	3.02	Spin-reorientation transition
fcc-Mn (Py)	3.16	Spin-reorientation transition
IrMn	3.01[38]	Exchange bias
MnPt	2.48[40]	Exchange bias

E. Magnetic anisotropy energies evaluated from phenomenological model

According to the analysis described above, we can extract, as shown in Fig. 6, the values of the total surface magnetic anisotropy energy ($K_s^0 + K_s^{\mathrm{Mn}}$) for both Fe/Mn and Py/Mn bilayers as functions of t_{Mn}. The values of $K_v t_{\mathrm{FM}}$ (where $K_v = K_{\mathrm{shape}} + K_{\mathrm{me}}$) for m ML Fe and m' ML Py are also indicated. For Fe/Cu_3Au(001) ($t_{\mathrm{Mn}} = 0$), the positive K_s^0 describes the perpendicular preference. However, as t_{Fe} is increased from low coverage to 4 ML, the negative $K_v t_{\mathrm{FM}}$ begins to overcome the positive K_s^0, leading to the SRT from the perpendicular to in-plane direction (see the crossover between the red solid and dotted lines at $t_{\mathrm{Mn}} = 0$). This leads to the invariant in-plane anisotropy for $t_{\mathrm{Fe}} > 4$ ML in Fe/Cu_3Au(001). Nevertheless, such SRT is not observed in Py/Cu_3Au(001) due to the intrinsic in-plane interface anisotropy (negative K_s^0). In both Fe/Mn and Py/Mn bilayers, the K_s^{Mn} shows positive values and enhances positively with the increase of t_{Mn}. This indicates that the Mn contributes PMA for both systems. Once t_{Mn} gets thicker, K_s^0 together with the positively enhanced K_s^{Mn} can overcome the negative K_v at specific t_{FM}, leading to the SRT from in-plane to perpendicular direction (as presented by triangular marks).

By comparing Fe/Mn and Py/Mn bilayers, we found that the ratio of $K_s^{\mathrm{Bulk\,Mn}}$ (~2.5) is close to the ratio of FM magnetic moment density ($M_{\mathrm{Fe}}/M_{\mathrm{Py}} \sim 2.18$). Such relationship can be interpreted by AFM-FM exchange coupling by applying the conventional exchange coupling formula $E \sim -J M_{\mathrm{FM}} M_{\mathrm{AFM}}$.[10] Assuming that Mn moments with PMA intrinsically at the interface exist, the Mn-FM exchange coupling energy becomes anisotropic for M_{FM} aligning in the in-plane and out-of-plane directions. Such energy difference gives rise to the interface anisotropy energy for the FM moments and could be the origin of K_s^{Mn}. Thus, this explains

TABLE II. The surface magnetic anisotropy energy of Fe and Py ultrathin films.

System	K_s^0 (μeV/atom)	K_s^0 (mJ/m^2)
bct Fe/Mn/Cu_3Au(001)	656.0 ± 15.2	1.70 ± 0.04
bcc Fe/Cu(001)[46]	725.7	1.88
fcc Fe/Cu(001)[47–49]	575.1	1.49
bcc Fe/Ag(001)[50]	540.4	1.40
bcc Fe/Ag(001)[51]	683.2	1.77
Free standing bcc Fe[52,53]	594.4	1.54
fct Py/Mn/Cu_3Au(001)	−68.5 ± 21.5	−0.177 ± 0.056
fct Py/Cu(001)[29,30]	−84.9	−0.220

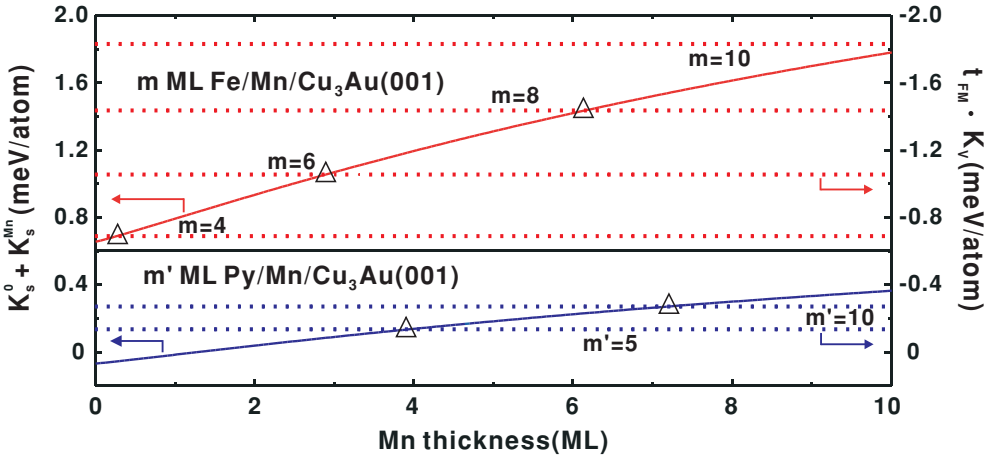

FIG. 6. (Color online) Magnetic anisotropy energies for the bilayered Fe/Mn/Cu_3Au(001) and Py/Mn/Cu_3Au(001) systems, simulated by the magnetic anisotropy model with finite-size scaling. The total surface magnetic anisotropy energy ($K_s^0 + K_s^{\mathrm{Mn}}$) for Fe/Mn and Py/Mn bilayers as a function of t_{Mn} is plotted by the red solid line and blue solid line, respectively (left axis). The values of $K_v t_{\mathrm{FM}}$ (where $K_v = K_{\mathrm{shape}} + K_{\mathrm{me}}$) for m ML Fe (red dotted line) and m' ML Py (blue dotted line) are also indicated (right axis). The SRT critical thickness is indicated by the open triangle marks in the crossover regions of $K_s^0 + K_s^{\mathrm{Mn}}$ and $K_v t_{\mathrm{FM}}$.

why the ratios of M_{FM} and $K_s^{\mathrm{Bulk\,Mn}}$ are close to each other within the Fe/Mn and Py/Mn bilayers. The small deviation may be due to the different Mn-FM exchange integral J in these two systems.

IV. DISCUSSION

A. Comparison between "conventional" interface anisotropy and interface anisotropy assisted by AFM-FM exchange coupling

In low-dimensional magnetic system like ultrathin film, the orbital moments at the surface or interface could be unquenched due to the broken symmetry. These unquenched orbital moments, which are correlated with the surface lattice and electronic structure, can give rise to the magnetic anisotropy of surface spin moments through the spin-orbital coupling. In some cases, the interface hybridization between FM layer and noble-metal layer can further enhance the out-of-plane oriented orbital moments at the interface and cause the large PMA. This is the origin of the PMA in Co/Pt or Co/Pd multilayer systems,[3,54–56] as well as of the thin Fe film/Cu_3Au(001).[18] Since such perpendicular interface anisotropy is commonly found in many low-dimensional magnetic systems, such as Fe/Ag(001),[57,58] Fe/Cu(100),[59,60] and Co/Au(111),[61] we called it "conventional" interface anisotropy (K_s^0) in order to distinguish it from the AFM-FM exchange coupling assisted interface anisotropy (K_s^{Mn}) in the present model [see Eq. (3)]. However, the PMA via such conventional interface anisotropy cannot be sustained as the FM film becomes thicker. This is because while the conventional interface anisotropy is independent of FM film thickness, the (in-plane) shape anisotropy plus magnetoelastic anisotropy increases proportionally with the thickness of FM film due to its volume characteristic. In the present case of Fe/Cu_3Au(001), it leads to the invariant in-plane magnetization as the Fe film becomes thicker than about 4 ML.

Apparently, both the conventional interface anisotropy (from interfacial electronic hybridization) and the interface anisotropy assisted by the AFM-FM exchange coupling belong to "interface" anisotropy. It is difficult to distinguish them by only varying the thickness of the FM layer. Since these two kinds of interface anisotropies are attributed to different physical origins, different (noble-metal and AFM-Mn) thickness-dependent characteristics are expected. Thus, we can distinguish them with this point. For thin Co/noble-metal multilayers, the PMA originates from the conventional interface anisotropy, mainly due to the interface (d-d) electronic hybridization between Co and noble metal.[3,54–56] The experiment findings show the characteristic that such hybridization is highly localized at the Co/Pt interface[3,55] and that the maximum magnitude for the PMA is often achieved when the noble metal has low coverage ($t_{\mathrm{Pt}} \sim 1$ ML).[4,56]

On the other hand, the AFM-FM exchange coupling is expected to be enhanced with the increase of AFM thickness. For the conventional AFM-FM exchange bias coupled systems,[10] although the unidirectional anisotropy (exchange bias) is considered as an interface effect, its magnitude (corresponding to exchange bias field or blocking temperature T_B) can still be enhanced with the increase of AFM thickness. This is owing to the exchange-coupled nature that the spins can interact with another spins within a certain range, described by the effective spin-correlation length ξ. Within such range, the increase of film thickness results in the more available exchange-coupled pairs (in the z direction) which contribute the larger exchange coupling energy to overcome the thermal energy. The strength of exchange coupling or T_B for AFM film finally saturates when its thickness approaches ξ, described by finite-size scaling.[11,12]

Following the above discussion, the effective spin-correlation length ξ, which is correlated with the exchange characteristic, should also be found in Fe(Py)/Mn/Cu_3Au(001), if the PMA truly originates from the AFM-FM exchange coupling and AFM exchange-coupled

nature. Indeed, according to the result of our modeling analysis, the ξ of the Mn layer in both the Fe/Mn and Py/Mn bilayers is ~16 ML (~3 nm). Such value is consistent with other Mn-based alloy films (see Table I) in exchange biased systems. The PMA enhanced monotonically until $t_{Mn} \sim 16$ ML is in sharp contrast to the expectation of conventional interface anisotropy ($t_{Pt} \sim 1$ ML), and thus one can exclude the conventional interface anisotropy as being the origin of enhanced PMA in Fe(Py)/Mn/Cu_3Au(001) systems.

B. Origin of PMA in FM/Mn/Cu_3Au(001)

On the other hand, as indicated in our results section, the crystalline structures of both FM layers remain invariant on the Mn underlayer even with different thicknesses or temperatures. Thus, the mechanism which causes the PMA in FM/Mn bilayers should be attributed to magnetic interaction rather than structural effects, for example, the crystalline anisotropy or magnetoelastic anisotropy. Indeed, as mentioned in our results and discussion, the PMA of both Fe/Mn and Py/Mn bilayers shows a finite-size tendency that the magnitude increases with t_{Mn} and finally saturates when the t_{Mn} approaches ~16 ML. This characteristic gives evidence of the AFM-FM exchange coupling as the origin of the PMA in FM/Mn bilayers. Moreover, such characteristic can also be observed in temperature-dependent experiments by measuring the thermal stability of the PMA of FM/Mn bilayers with varying t_{Mn}. In Fig. 7(a), the 6 ML Fe/6 ML Mn bilayer exhibits PMA at low temperature. As the temperature is elevated, its magnetization switches from the perpendicular to in-plane direction with a transition temperature $T_{SRT} \sim 230$ K. This temperature-dependent SRT is also seen in 6 ML Fe/8 ML Mn at a higher $T_{SRT} \sim 245$ K [Fig. 7(b)]. The variation of T_{SRT} is plotted as a function of t_{Mn} in Fig. 7(c), in which T_{SRT} increases monotonically from 220 K to 245 K as t_{Mn} is raised from 2 ML to 8 ML. Similarly to T_B, which describes the strength of "pinned" uncompensated spins in exchange bias coupled systems,[37,62] T_{SRT} in this work can also be used to monitor the thermal stability of the "effective" magnetic ordering in the AFM Mn layer which is associated with the established PMA of Fe/Mn bilayers. Thus, in Fig. 7(c) the T_{SRT} monotonic increase with AFM thickness reveals the same finite-size effect tendency as found in T_B for the AFM-FM exchange bias systems.[12,38] Such tendency again distinguishes the present coupling type from the spin-orbital coupling at interfaces that supports the conventional perpendicular interfacial (magnetocrystalline) anisotropy in FM/noble-metal bilayers or multilayers, because the latter case presents the maximum strength of PMA for noble-metal thickness with low coverage ($t_{Pt} \sim 1$ ML for Co/Pt).[4,56]

Furthermore, we have pointed out that the value of $K_s^{\text{Bulk Mn}}$ shows a ratio of ~2.5 between Fe/Mn and Py/Mn systems. This ratio is close to the value (~2.18) of M_{Fe}/M_{Py} and can be explained by the AFM-FM exchange coupling within the model of $E \sim -J M_{FM} M_{AFM}$.[10] This may imply that the localized Mn moments existed near the FM/Mn interface. Indeed, Mn moments with localized characteristics have been found in Mn thin film systems[63–65] and may originate from the dominance of their 3*d* valence electrons with localized preference.[64] Although the direct measurement of the magnetic configuration of the fcc-Mn layer has not been achieved, Hafner and Spišák found spin spiral solutions at the X and L points for fcc-Mn.[65] The latter solution, which corresponds to the [111] layered AFM structure, suggests the possible existence of out-of-plane spin moments which may be responsible for the PMA in FM/Mn bilayer systems.

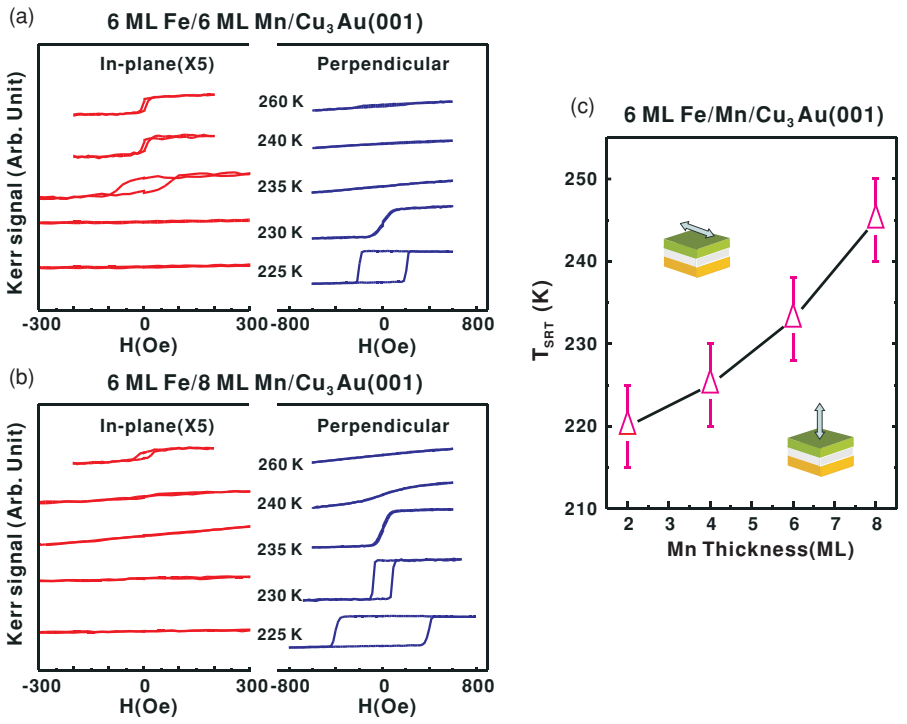

FIG. 7. (Color online) Temperature-dependent hysteresis loops for (a) 6 ML Fe/6 ML Mn/Cu_3Au(001) and (b) 6 ML Fe/8 ML Mn/Cu_3Au(001). (c) The spin reorientation transition temperature (T_{SRT}) for 6 ML Fe/Mn/Cu_3Au(001) as a function of t_{Mn}.

C. Comparison of perpendicular anisotropy energy assisted by AFM-FM exchange coupling and exchange bias coupling energy

In the present work, the PMA found in FM/Mn bilayers is driven by the AFM-FM exchange coupling, but not directly correlated and described by exchange bias energy. This is because exchange bias energy describes the unidirectional anisotropy energy along the easy axis or a certain external field axis ($+H$ and $-H$ field direction) and does not count the energy difference between the two different magnetization axes, for example, the in-plane and perpendicular directions in our case [Eq. (1)]. According to the review articles on exchange bias coupling,[10,66] the magnitude of exchange bias energy can be described in terms of interface energy per unit area ΔE:

$$\Delta E = M_{\mathrm{FM}} t_{\mathrm{FM}} H_E, \tag{4}$$

where M_{FM} and t_{FM} are the saturation magnetization and thickness of the ferromagnet and H_E is the exchange bias magnitude. Conventionally, the exchange bias field is defined as $H_E = (H_{C+} - H_{C-})/2$, where H_{C+} and H_{C-} are corresponding to the positive and negative coercive field, respectively. As a result, ΔE is rewritten as

$$\Delta E = \tfrac{1}{2}(M_{\mathrm{FM}} t_{\mathrm{FM}} H_{C+} - M_{\mathrm{FM}} t_{\mathrm{FM}} H_{C-}) = \tfrac{1}{2}(E_+ - E_-), \tag{5}$$

where E_+ and E_- are the Zeeman energies requested for aligning the magnetization to the positive and negative direction, respectively, via external fields. ΔE is proportional to the energy difference between E_+ and E_-. On the other hand, the perpendicular anisotropy energy required for a perpendicular magnetization is defined as the relative energy difference between those with the in-plane and perpendicular magnetization [see Eq. (1)]. Therefore, both energies (with different definitions) give similar concepts of relative value rather than an absolute one.

In the present work, the energy values observed to support the PMA in FM/Mn bilayers can be up to several meV/atom. Such energy is much larger than the exchange bias energy for Mn-based alloy from the literature[10,67] ($\sim$100 μeV/atom). However, this "discrepancy" will not affect the possible existence of a perpendicular easy axis due to the AFM-FM exchange coupling because of the different definitions. The energy value of PMA can be larger than the exchange bias coupling one, even when they have similar physical origins (AFM-FM exchange coupling). It is noted that our perpendicular anisotropy energy has values the same as or even larger than those reported by previous studies with the conventional interfacial anisotropy due to spin-orbital coupling[68,69] (see Fig. 6 and Table II).

V. CONCLUSION

In conclusion, we have demonstrated a mechanism leading to PMA in FM ultrathin films by AFM-FM exchange coupling. The evidences includes (i) the enhancement of H_c with AFM thickness as a fingerprint of AFM-FM exchange coupling;[10] (ii) the extension of the FM thickness range for PMA and the monotonic increased thermal stability of PMA (T_{SRT}) with AFM thickness, as the modulation of AFM-FM exchange coupling due to the finite-size effect of the AFM layer[12,38] (both phenomena are in sharp contrast to the tendency of "conventional" interfacial anisotropy); (iii) quantitative analysis of the phase diagrams that takes finite-size effects into account in the phenomenological model, and the strength of PMA following $E \sim -J M_{\mathrm{FM}} M_{\mathrm{AFM}}$ when comparing Fe/Mn and Py/Mn bilayers. AFM-FM coupling is one of the most investigated features of magnetism. Our work demonstrates its critical impact on PMA, in addition to the well-known exchange bias behavior. This may lead to the PMA desired at the frontier of recording technology.

ACKNOWLEDGMENTS

This work was supported in part by the National Science Council of Taiwan through Grant No. NSC 98-2120-M-002-010. M. T. Lin would like to thank the NSRRC Nanomagnetism Program for the support of the NSRRC-NTU Nanomagnetism Chamber at PEEM Endstation.

*mtlin@phys.ntu.edu.tw

[1] D. Weller and A. Moser, IEEE Trans. Magn. **35**, 4423 (1999).
[2] S. Mangin, D. Ravelosona, J. A. Katine, M. J. Carey, B. D. Terris, and E. E. Fullerton, Nature Mater. **5**, 210 (2006).
[3] N. Nakajima, T. Koide, T. Shidara, H. Miyauchi, H. Fukutani, A. Fujimori, K. Iio, T. Katayama, M. Nývlt, and Y. Suzuki, Phys. Rev. Lett. **81**, 5229 (1998).
[4] M. T. Johnsony, P. J. H. Bloemenzx, F. J. A. den Broeder, and J. J. de Vries, Rep. Prog. Phys. **59**, 1409 (1996).
[5] B. Schulz and K. Baberschke, Phys. Rev. B **50**, 13467 (1994).
[6] W. C. Lin, B. Y. Wang, Y. W. Liao, K. J. Song, and M. T. Lin, Phys. Rev. B **71**, 184413 (2005).
[7] B. Y. Wang, W. C. Lin, Y. W. Liao, K. J. Song, and M. T. Lin, Surf. Sci. **600**, 4517 (2006).
[8] A. Winkelmann, M. Przybylski, F. Luo, Y. Shi, and J. Barthel, Phys. Rev. Lett. **96**, 257205 (2006).
[9] S. Mao, Z. Gao, H. Xi, P. Kolbo, M. Plumer, L. Wang, A. Goyal, I. Jin, J. Chen, C. Hou, R. M. White, and E. Murdock, IEEE Trans. Magn. **38**, 26 (2002).
[10] J. Nogués and I. K. Schuller, J. Magn. Magn. Mater. **192**, 203 (1999).
[11] T. Ambrose and C. L. Chien, Phys. Rev. Lett. **76**, 1743 (1996).
[12] S. K. Mishra, F. Radu, S. Valencia, D. Schmitz, E. Schierle, H. A. Dürr, and W. Eberhardt, Phys. Rev. B **81**, 212404 (2010).
[13] S. M. Zhou, L. Sun, P. C. Searson, and C. L. Chien, Phys. Rev. B **69**, 024408 (2004).
[14] H. Xing, K. Keshoju, S. M. Zhou, and L. Sun, J. Appl. Phys. **101**, 09E509 (2007).
[15] See further discussion in Sec. IV C.
[16] W. C. Lin, T. Y. Chen, L. C. Lin, B. Y. Wang, Y. W. Liao, K. J. Song, and M. T. Lin, Phys. Rev. B **75**, 054419 (2007).

[17]W. C. Lin, C. C. Kuo, C. L. Chiu, and M. T. Lin, Surf. Sci. **478**, 9 (2001).
[18]M. T. Lin, J. Shen, W. Kuch, H. Jenniches, M. Klaua, C. M. Schneider, and J. Kirschner, Phys. Rev. B **55**, 5886 (1997).
[19]M. T. Lin, J. Shen, W. Kuch, H. Jenniches, M. Klaua, C. M. Schneider, and J. Kirschner, Surf. Sci. **410**, 290 (1998).
[20]B. Feldmann, B. Schirmer, A. Sokoll, and M. Wuttig, Phys. Rev. B **57**, 1014 (1998).
[21]F. Bruno, S. Terreni, L. Floreano, A. Cossaro, D. Cvetko, P. Luches, L. Mattera, A. Morgante, R. Moroni, M. Repetto, A. Verdini, and M. Canepa, Phys. Rev. B **66**, 045402 (2002).
[22]S. H. Lu, J. Quinn, D. Tian, F. Jona, and P. M. Marcus, Surf. Sci. **209**, 364 (1989).
[23]R. Rochow, C. Carbone, Th. Dodt, F. P. Johnen, and E. Kisker, Phys. Rev. B **41**, 3426 (1990).
[24]P. Luches, A. D. Bona, S. Valeri, and M. Canepa, Surf. Sci. **471**, 32 (2000).
[25]J. Stöhr, Y. Wu, B. D. Hermsmeier, M. G. Samant, G. R. Harp, S. Koranda, D. Dunham, and B. P. Tonner, Science **259**, 658 (1993).
[26]C. M. Schneider and G. Schönhense, Rep. Prog. Phys. **65**, R1785 (2002).
[27]F. Bisio, S. Terreni, G. Gonella, L. Floreano, A. Morgante, M. Canepa, and L. Mattera, Phys. Rev. Lett. **93**, 106103 (2004).
[28]P. M. Marcus and F. Jona, Surf. Rev. Lett. **1**, 15 (1994).
[29]R. Thamankar, A. Ostroukhova, and F. O. Schumann, Phys. Rev. B **66**, 134414 (2002).
[30]P. Weinberger, L. Szunyogh, C. Blaas, C. Sommers, and P. Entel, Phys. Rev. B **63**, 094417 (2001).
[31]L. Néel, Comptes Rendus **237**, 1468 (1953); J. Phys. Radium **15**, 225 (1954).
[32]J. A. C. Bland and B. Heinrich, *Ultrathin Magnetic Structures* (Springer-Verlag, Berlin, 1994), Vol. 1.
[33]F. Huang, G. J. Mankey, M. T. Kief, and R. F. Willis, J. Appl. Phys. **73**, 6760 (1993).
[34]R. Zhang and R. F. Willis, Phys. Rev. Lett. **86**, 2665 (2001).
[35]E. Weschke, H. Ott, E. Schierle, C. Schüßler-Langeheine, D. V. Vyalikh, G. Kaindl, V. Leiner, M. Ay, T. Schmitte, and H. Zabel, Phys. Rev. Lett. **93**, 157204 (2004).
[36]P. J. van der Zaag, Y. Ijiri, J. A. Borchers, L. F. Feiner, R. M. Wolf, J. M. Gaines, R. W. Erwin, and M. A. Verheijen, Phys. Rev. Lett. **84**, 6102 (2000).
[37]Y. Ijiri, T. C. Schulthess, J. A. Borchers, P. J. van der Zaag, and R. W. Erwin, Phys. Rev. Lett. **99**, 147201 (2007).
[38]A. J. Devasahayam and M. H. Kryder, J. Appl. Phys. **85**, 5519 (1999).
[39]H. Xi, R. M. White, Z. Gao, and S. Mao, J. Appl. Phys. **92**, 4828 (2002).
[40]M. Rickart, A. Guedes, J. Ventura, J. B. Sousa, and P. P. Freitas, J. Appl. Phys. **97**, 10K110 (2005).
[41]See further discussion in Sec. IV A.
[42]M. Henkel, S. Andrieu, P. Bauer, and M. Piecuch, Phys. Rev. Lett. **80**, 4783 (1998).
[43]P. James, O. Eriksson, B. Johansson, and I. A. Abrikosov, Phys. Rev. B **59**, 419 (1999).
[44]T. Burkert, O. Eriksson, P. James, S. I. Simak, B. Johansson, and L. Nordström, Phys. Rev. B **69**, 104426 (2004).
[45]W. Schweika, D. P. Landau, and K. Binder, Phys. Rev. B **53**, 8937 (1996).
[46]D. E. Fowler and J. V. Barth, Phys. Rev. B **53**, 5563 (1996).
[47]D. Peterka, A. Enders, G. Haas, and K. Kern, Phys. Rev. B **66**, 104411 (2002).
[48]B. Heinrich, Z. Celinski, J. F. Cochran, A. S. Arrott, and K. Myrtle, J. Appl. Phys. **70**, 5769 (1991).
[49]U. Gradmann, in *Handbook of Magnetic Materials*, edited by K. H. J. Buschow (Elsevier Science B. V., North-Holland, 1993), Vol. 7.
[50]R. J. Hicken, S. J. Gray, A. Ercole, C. Daboo, D. J. Freeland, E. Gu, E. Ahmad, and J. A. C. Bland, Phys. Rev. B **55**, 5898 (1997).
[51]B. Heinrich and J. F. Cochran, Adv. Phys. **42**, 523 (1993).
[52]J. G. Gay and R. Richter, Phys. Rev. Lett. **56**, 2728 (1986).
[53]J. G. Gay and R. Richter, in *Ultrathin Magnetic Structures*, edited by J. A. C. Bland and B. Heinrich (Springer-Verlag, Berlin, 1994), vol. 1, p. 21.
[54]D. Weller, A. Carl, R. Savoy, T. C. Huang, M. F. Toney, and C. Chappert, J. Phys. Chem. Solids **56**, 1562 (1995).
[55]Y. Wu, J. Stöhr, B. D. Hermsmeier, M. G. Samant, and D. Weller, Phys. Rev. Lett. **69**, 2307 (1992).
[56]N. Sato, J. Appl. Phys. **64**, 6424 (1988).
[57]D. Li, M. Freitag, J. Pearson, Z. Q. Qiu, and S. D. Bader, Phys. Rev. Lett. **72**, 3112 (1994).
[58]J. Thomassen, F. May, B. Feldmann, M. Wuttig, and H. Ibach, Phys. Rev. Lett. **69**, 3831 (1992).
[59]Z. Q. Qiu, J. Pearson, and S. D. Bader, Phys. Rev. Lett. **70**, 1006 (1993).
[60]J. A. C. Bland, A. D. Johnson, R. D. Bateson, and H. J. Lauter, J. Magn. Magn. Mater. **104–107**, 1798 (1992).
[61]R. Allenspach, M. Stampanoni, and A. Bischof, Phys. Rev. Lett. **65**, 3344 (1990).
[62]H. Ohldag, H. Shi, E. Arenholz, J. Stöhr, and D. Lederman, Phys. Rev. Lett. **96**, 027203 (2006).
[63]U. Schlickum, N. Janke-Gilman, W. Wulfhekel, and J. Kirschner, Phys. Rev. Lett. **92**, 107203 (2004).
[64]I. Di Marco, J. Minár, S. Chadov, M. I. Katsnelson, H. Ebert, and A. I. Lichtenstein, Phys. Rev. B **79**, 115111 (2009).
[65]J. Hafner and D. Spišák, Phys. Rev. B **72**, 144420 (2005).
[66]W. H. Meiklejohn, J. Appl. Phys. **33**, 1328 (1962).
[67]W. C. Lin, T. Y. Chen, L. C. Lin, B. Y. Wang, K. J. Song, and M. T. Lin, Appl. Phys. Lett. **90**, 052502 (2007).
[68]B. N. Engel, C. D. England, R. A. Van Leeuwen, M. H. Wiedmann, and C. M. Falco, Phys. Rev. Lett. **67**, 1910 (1991).
[69]Z. Zhang, P. E. Wigen, and S. S. P. Parkin, J. Appl. Phys. **69**, 5649 (1991).